Materials Science for Energy Technologies 5 (2022) 99–109

Contents lists available at ScienceDirect

Materials Science for Energy Technologies

journal homepage: www.keaipublishing.com/en/journals/materials-science-for-energy-technologies

Nano-sized mesoporous biochar derived from biomass pyrolysis as electrochemical energy storage supercapacitor

Zakir Husain [a,b,1], Shakeelur Raheman A.R. [c,1], Khursheed B. Ansari [d,*], Aniruddha B. Pandit [a,*], Mohd Shariq Khan [e], Muhammad Abdul Qyyum [f], Su Shiung Lam [g,h]

[a] Department of Chemical Engineering, Institute of Chemical Technology, Mumbai, Maharashtra 400019, India
[b] Department of Civil Engineering, Indian Institute of Technology, Gandhinagar, Gujarat 382355, India
[c] Department of Applied Science, Shri Vile Parle Kelavani Mandal's Institute of Technology, Dhule, Maharashtra 424001, India
[d] Department of Chemical Engineering, Zakir Husain College of Engineering and Technology, Aligarh Muslim University, Aligarh, Uttar Pradesh 202001, India
[e] Department of Chemical Engineering, College of Engineering, Dhofar University, Salalah 211, Sultanate of Oman
[f] Department of Petroleum & Chemical Engineering, Sultan Qaboos University, Muscat, Oman
[g] Higher Institution Centre of Excellence (HICoE), Institute of Tropical Aquaculture and Fisheries (AKUATROP), Universiti Malaysia Terengganu, Kuala Nerus, Terengganu 21030, Malaysia
[h] Henan Province Forest Resources Sustainable Development and High-value Utilization Engineering Research Center, School of Forestry, Henan Agricultural University, Zhengzhou 450002, China

ARTICLE INFO

Article history:
Received 26 October 2021
Revised 12 December 2021
Accepted 16 December 2021
Available online 22 December 2021

Keywords:
Biomass pellets
Pyrolysis
Nano-sized biochar
Characterization
Pseudo capacitance
Electrochemical performance

ABSTRACT

Energy storage is essential to conserve and deliver energy to end-user with continuity and durability. A sustainable energy supply with minimal process losses requires cost-effective and environmentally friendly energy storage material. In this study, self-co-dopes N (3.65 %) and O (6.44 %) porous biochar were produced from pyrolysis of biomass pellets (made from garden wastes) and examined for energy storage application. The presence of co-doped-heteroatoms within the carbon matrix of biochar resulted in enhanced surface wettability, fast charge transfers, increased electrical conductivity, and low internal resistance. Biochar produced at 800 ℃ (i.e. biochar-800) showed desirable pseudocapacitive nature induced by self-co-doped heteroatoms. Two-electrode measurements in aqueous 1 M H_2SO_4 revealed that biochar-800 possessed 228F g^{-1} of specific capacitance at a current density of 1 Ag^{-1} Additionally, biochar-800 exhibited a high energy density of 7.91 Wh kg^{-1} in aqueous electrolyte and promising cycling stability with 88% capacitance retention after 5000 cycles at 10 A g^{-1}. Enhanced capacitive performance of biochar-800 was assigned to the presence of self-co-doped heteroatom, the high specific surface area of 312 m^2g^{-1}, and self-formed mesopores (pore size around 15.2 nm). This study demonstrates the great promise of porous biochar derived from biomass pellets as a low-cost electrode material for high-performance energy storage devices.

1. Introduction

The growing population and industrial energy demand, depleting traditional fossil fuels, and deteriorating environment have prompted efforts to look for sustainable energy and storage [1]. Nowadays, batteries and supercapacitors are widely used as energy storage devices. Large amounts of energy can be stored in metal-air [2], sodium-sulfur [3], and lithium-ion batteries [4], which can later be utilized when needed. Most batteries, however, work on the electrochemical cycle and hence depend on the electrode and electrolyte materials for their efficiency. Compared to the electrochemical cycle-based batteries, the supercapacitor is electrostatically controlled and shows promising features in operation and sustainability [5,6]. In the context of performance, supercapacitor holds several advantages over batteries, such as high power capacity, fast charging/discharging from several thousand to millions of cycles, but it has the constraint of low energy density [7]. Several nanostructured materials such as graphene [8,9], carbon nanotubes (CNT) [8,10], carbon nanosheets [11], graphene quantum

* Corresponding authors.
E-mail addresses: akabadruddin@myamu.ac.in (K.B. Ansari), ab.pandit@ictmumbai.edu.in (A.B. Pandit).
[1] Zakir Husain and Shakeelur Rahman A.R have contributed equally to this work.
Peer review under responsibility of KeAi Communications Co., Ltd.

Production and hosting by Elsevier

https://doi.org/10.1016/j.mset.2021.12.003
2589-2991/

dots (GQDs) [12], porous and mesoporous carbon [13], 3-D graphene sponge, and foam [14] are explored to increase the efficiency of supercapacitor. Notably, it is easy to produce and characterize the nano-materials mentioned above on the laboratory scale; however, due to the high price of precursor and related tedious synthesis process, nano-material production at a large scale remains challenging. Also, the manufacturing cost of nano-materials is reported to be high (≈ $150 – $200 per kg) [15]. As an alternative, a potentially cheaper biomass-based nano-sized biochar would be more attractive in this scenario (i.e., coconut shell-derived biochar as supercapacitor material, $5 – $40 per kg) [15]. Similarly, metal oxide and conducting polymer-based supercapacitor possess an advantage over biochar-based supercapacitors due to high specific capacitance and pseudocapacitive nature. However, metal oxide suffers in electrical conductivity while conducting polymers experience a gradual loss of capacitive performance [16–18]. It is a known fact that the most critical component for the supercapacitor is the electrode material, which determines its performance. Therefore, the emerging field of supercapacitor research is manufacturing cost-effective and high-performance materials using an easy synthesis method applicable on a large scale [7,19].

A detailed literature review reveals that biomass-derived biochar can be an electrode material for charge storage applications [7,20–22]. Moreover, biomass-derived products can be utilized for energy generation and storage [7,23,24]. The different biomass-based precursors, viz. cellulose, orange peel, coconut-shell, corncob, peanut shells, carbon stalk, have been investigated for their conversion into supercapacitor material (or biochar) because of their abundant availability, cost-effectiveness, and renewable nature [19,25–29]. Moreover, the biochar showed a unique microstructure, good electrical conductivity, high specific surface area (800–3012 m^2g^{-1}), and the chemical composition comprising natural self-doped heteroatoms [7,30–32]. The naturally embedded heteroatoms in the biochar structure, i.e., nitrogen (N), sulfur (S), phosphorus (P), calcium (Ca), play an essential role as an electron donor, maintaining surface hydrophilicity and excellent cyclic stability [33–38]. Further, the hetero-atoms improve carbon wettability, electron conductivity, and basic strength, inducing pseudo-capacitive behavior [7]. The synergistic effect of the pore structure, which is due to unique feedstock (biomass) microstructure and rich heteroatoms, makes the self-doped biochar a potential candidate for the energy storage device [39].

Xu et al. performed the carbonization of gelatin (an animal derivative) under an inert atmosphere to make self-doped biocarbon (specific surface area ≈ 3012 m^2g^{-1}) and test for supercapacitor application [40]. The nitrogen on the carbon surface remained the most common mono-heteroatom, which was further classified into four standard forms, such as pyridine-N (N-6), pyrrolic/pyridine-N (N-5), quaternary- N (N-Q), and oxidized pyridine-N (N-X) [41]. Consequently, in multiple heteroatom co-doping, carbon materials comprised O-N-S heteroatoms [41]. Numerous research has shown the potential of O-N-S co-doped hierarchical porous carbon for use as supercapacitor electrodes (summarize in Chen et al., 2019) [2,42,43]. Compared to mono-heteroatom doping, carbon with multi-heteroatom doping showed a higher specific capacity [43].

The literature suggests that biochar prepared from the pyrolysis of biomass precursors (e.g., agricultural waste, wood residue, and manure) hold a hierarchical porous structure and remain promising for supercapacitor applications [44,45]. Wang et al. demonstrated that Ni-loaded biochar prepared from dairy manure and sewage sludge pyrolysis could be a good supercapacitor material with 123 Fg^{-1} specific capacitance [46]. The specific capacitance of biochar was reduced by only 2% after 1000 charge-discharge cycles. In another report, the biochar prepared from the carbonization of southern yellow pine sawdust was utilized as an anode electrode material in the supercapacitor [47]. The capacitor exhibited the specific capacitance of 21 Fg^{-1} at 5 mV s^{-1} along with no decay in performance after 1000 cycles. The Bamboo fibers were prepared using two-step carbonization (viz. hydrothermal treatment at 180 °C in acidic media followed by pyrolysis at 800 °C under Argon atmosphere indicated a high specific capacitance of 510 Fg^{-1} at 0.4 A g^{-1} [45]. Further, it showed excellent charge storage stability over 5000 charge-discharge cycles. Furthermore, following gamma radiation, the biomass-derived biochar demonstrated enhanced supercapacitor performance [48]. After gamma irradiation (dose of 100 kGy), the biochar showed higher specific capacitance (246.2 Fg^{-1}) than the untreated biochar (115.3 Fg^{-1}). Additionally, the biochar depicted around 96% capacity retention for 10,000 cycles at 2 Ag^{-1} because of its particle size and enhanced porosity (after irradiation). The hollow tubular-like porous carbon (HT-PC) was prepared from the biomass (or waste feather finger grass flower) carbonization (via pyrolysis at 550 °C followed by acid wash and drying) [49]. HT-PC indicated the highest specific capacitance of 315 Fg^{-1} at 1 Ag^{-1} and retained 96% of its capacitance after 50,000 cycles. The supercapacitor features of the biochar remained strongly dependant on the biomass sources and the preparation methods. The reports on nano-sized biochar prepared from garden waste biomasses are rarely available in the literature to the best of our knowledge. Therefore, the current research is aimed to produce nano-sized biochar (from the waste garden biomass material or biomass pellet) equipped with a high energy density for supercapacitor applications. This work explicitly utilized biochar (one of the byproducts of the biomass pyrolysis process) and demonstrated its potential for use as an energy storage material for supercapacitors. The biochar containing heteroatoms were prepared at 600 ℃ and 800 ℃ and named biochar-600 and biochar-800, respectively. The ability of the biochar as a supercapacitor was evaluated by extensive characterization such as X-ray diffraction (XRD), Raman spectroscopy, energy-dispersive X-ray (EDX), transmission electron microscopy (TEM), BET surface area analysis, and X-ray photon spectroscopy. Additionally, the biochar's cyclic voltammetry and specific capacitance measurements were performed at various current densities to evaluate its capacitance, cyclic stability, and energy storage capacity.

2. Experimental section

The preparation of biomass pellets from garden biomass waste and biomass-derived biochar formation is shown in Fig. 1[A] and discussed below.

2.1. Preparation of biomass pellet

The following steps were involved in the preparation and production of biomass pellets from garden waste:

(i) Collection of biomass such as wood straw, chips, grass, and garden waste (ii) Size reduction of biomass in a crusher/shredder to achieve it in the form of powder (particle size ≈ 1 – 4 mm) (iii) Addition of water to the shredded biomass for the process of lignin melting that served as a binder (iv) Transformation of biomass powder into pellets (dia. 8 – 10 mm and length 15 – 35 mm) in a Pellet Maker PM-125 machines (Fig. 1[A]). The biomass pellet density and moisture content were estimated at 1100–1300 kg^{-1} m^3 and 7 – 10 wt%, respectively.

2.2. Production of biochar

The dried biomass pellets (i.e., 10gm) with an initial moisture content of 7 wt% was placed in the quartz boat for the pyrolysis process. The pyrolysis of biomass pellets was conducted in a tubu-

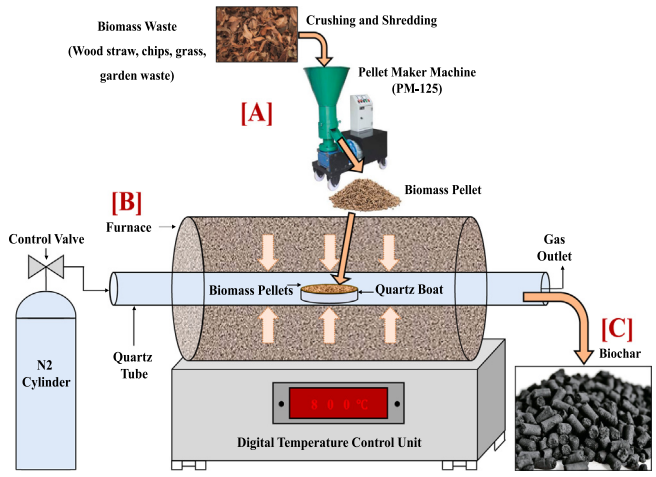

Fig. 1. [A] Preparation of biomass pellets [B] Preparation of biomass-derived biochar [C] Camera image of biomass-derived biochar (biochar-800).

lar quartz reactor at 600 ℃ and 800 ℃ at constant heating rate 5 °C/min to convert it into biochar (Fig. 1[B]) During the pyrolysis process nitrogen (N) gas at a 100 ml/min flow rate was supplied to maintain the inert atmosphere. Pyrolysis vapors were released by the thermal decomposition of biomass pellets, which instantly left the reactor system because of the constant sweeping by the inert nitrogen gas, leaving behind carbonaceous biochar as the final product. The product samples (i.e., biochar-600 and biochar-800) were collected from the reactor at the end of the operation. Finally, to obtain the nano-sized carbon sheet within biochar, the collected biochar-600 and biochar-800 were crushed in mortar-pestle, dispersed in an ethanol solution, and kept for 6 h in an ultrasonic bath. The biochar-800 image is shown in Fig. 1[C]. The biochar samples were then employed to fabricate a coin cell for the two-electrode system, which is discussed in the next section.

2.3. Fabrication of cell for two-electrode measurement

The two-electrode coin cell used to fabricate the supercapacitor is depicted in Fig. S1 (supporting information). The electrode material was prepared by adding 90 wt% of biochar (in powder form), 5 wt% acetylene black, and 5 wt% polyvinylidene fluoride (PVDF) into the 2 ml N-Methyl-2-pyrrolidone (NMP) followed by bath sonication to form the uniform slurry. The current collector (i.e., conducting carbon sheet) was weighed before and after the material deposition to control the electrode material's mass loading. Besides the two conducting carbon sheets, the slurry of the electrode material was spin-coated evenly, followed by drying at 60 °C in the vacuum oven. Mass loading of 1.5 mg was uniformly deposited on each electrode with a surface area of 0.9 cm^2. An electrolyte-soaked glass fiber separator (Whatman) was placed between these two electrodes, and the supercapacitor cell was assembled in the CR2032 type coin cell. All electrochemical measurements were conducted on the CHI-302 N electrochemical workstation. In 1 M H_2SO_4, cyclic voltammetry (CV) measurements were performed in the range of 0 V to 1 V by varying the scan rate in 5 mVs^{-1} to 150 mVs^{-1}. The H_2SO_4 was selected as an electrolyte over KOH (potassium hydroxide) or KNO_3 (potassium nitrite) electrolytes because of its smaller ions size, which readily enters into the electrode pores and thus helps in enhancing the electrochemical energy storage performance. Further, the galvanostatic charge–discharge (GCD) measurement was conducted in the range of 1 Ag^{-1} to 10 Ag^{-1} and over a voltage range of 0 V to 1 V. Further, the electrochemical impedance spectroscopy test was conducted with an A.C. amplitude of 10 mV in the frequency range of 10 kHz to 10 mHz.

For quantitative purposes, in the two-electrode symmetric cell, the specific capacitance (C_S) of the electrode was measured from the charge–discharge curve value using the equation (1) [50].

$$C_s = \frac{2 \times I\Delta t}{m\Delta v} \quad (1)$$

$C_s$denotes the specific capacitance of electrode in (F g^{-1}); I (A) represents the constant discharge current, 'm' indicates the mass of active material loaded on one of the electrodes, and Δv signifies the potential change in (V) within the discharge time Δt (in second). The energy density of the supercapacitor was calculated by using equation (2).

$$E = \frac{1}{2} C_s V^2 \quad (2)$$

2.4. Characterization of biochar

The detailed characterization of biochar for its potential as a supercapacitor is discussed below.

- ***The crystallinity of biochar:*** Using the powder X-Ray diffraction technique (XRD), the prepared biochar's crystalline nature was determined, and the patterns were reported using CuKα radiation (a = 1.54 Å) in BRUKER D8 ADVANCE.
- ***Surface morphology of biochar:*** The surface morphology and structures of biochar samples were characterized using higher-resolution transmission electron microscopy (HR-TEM). JEM 2100F by JEOL instrument was used to measure particle size and dispersion of biochar with an operating voltage of 200 kV.
- ***Surface area and pore structure analysis of biochar:*** Brunauer-Emmett-Teller (BET) technique was used for the specific surface area measurement of biochar samples in a SMART SORM 93 instrument. The pore size distributions were calculated using the Barrett-Joyner-Halenda (BJH) method. Moreover, BRUKER RFS 27 Standalone FT-Raman Spectrometer was used to understand the scattering center of a porous structure of biochar samples with a spectral range of 4000–50 cm^{-1} using Nd: YAG 1064 nm LASER source.
- ***Surface chemical composition of biochar:*** The surface composition of biochar samples was determined through X-ray photoelectron spectroscopy (XPS) on a PHI 5000 Versa Probe III (by physical electronics) with a monochromatic, micro-focused, scanning x-ray source.

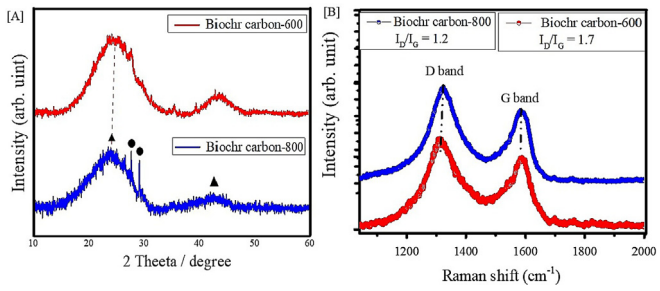

Fig. 2. Characterization of biochar via [A] X-Ray Diffraction and [B] Raman spectroscopy.

3. Result and discussion

3.1. X-ray diffraction analysis of biochar

The results on X-ray diffraction (XRD) analysis of biochar-600 and biochar-800 samples are shown in Fig. 2[A]. The 2θ values of XRD measurement are found in the range of 10° to 60° at 0.02^0 steps with a count time of 0.2 s. The diffraction peak intensity at angle 2θ values of 25.8° and 43.7° are assigned to (002) well-developed graphitic stacking and (100) reflection of the disordered carbon layer, respectively. With an increase in the pyrolysis temperature, the intensity of peaks (002) and (100) of biochar-800 sample decreased, referring to the graphitic structure of amorphous carbon [51]. Furthermore, the diffraction peak intensity at 43.7° of biochar-800 is reduced at a higher temperature, confirming pore formation within the material [52]. In the case of biochar-800, the diffraction peak intensity at 28.1° was due to inorganic components (SiO_2) within the biomass collected from the garden. The diffraction peak intensity at 29.4° revealed $CaCO_3$ due to the presence of the minerals in natural biomass [53].

3.2. Raman spectroscopy analysis of biochar

Raman spectroscopy was performed to analyze the defects and nature of the disorder within the biochar materials. In Fig. 2[B], the spectra for biochar-600 and biochar-800 show the peaks at nearly 1317 $cm^{-1}$and 1327 cm^{-1} are assigned to the D band (disorder sp^2 hybridized carbon atoms of graphite and defect site). The peaks located at 1581 cm^{-1} and 1583 cm^{-1} are G band which corresponds to the phonon mode in-plane vibration of sp^2 bonded carbon atom and serve as graphitic carbon fingerprints. The D and G bands' intensity ratio (I_D/I_G) reflects the degree of disorder in the carbon material [54]. Herein biochar-800 shows the comparatively lower I_D/I_G ratio of 1.2 than biochar-600 (I_D/I_G ratio of 1.7), which is assigned to the high density of disorder and defects in biochar-600 [55]. As a result, the biochar-800 has low sp^3 amorphous carbon rather than nanocrystalline graphite, which is consistent with the XRD results [56].

3.3. Surface area analysis of biochar

The surface area and porosity are the essential properties of biochar to assess its capacitive performance. Fig. 3[A] shows the N_2 adsorption/desorption isotherm analysis of biochar samples at various temperatures, which demonstrates a type I and type II pattern for relative pressure P/P_0 and high P/P_0 with an appropriate H_4 hysteresis loop [57,58]. The biochar samples showed a certain amount of N_2 adsorption below the relative pressure P/P_0 (less than 0.1), suggesting the presence of a mesoporous structure. The increase in relative pressure beyond $P/P_0 > 0.9$ reflected the integral porosity in biochar samples, caused by the interspace between the carbon layer, which provided the sufficient mesopores channel to access the electrolyte [58]. The biochar sample obtained at the higher temperature, i.e., biochar-800, exhibited an enhanced porous structure than the biochar-600, which was also revealed by the TEM image in Fig. S2. Further, the BET surface area of the biochar-800 showed a higher value of 312 m^2g^{-1} than the biochar-600 (99.1 m^2g^{-1}). Thus, an increase in activation temperature contributed to an increase in the capacity to generate narrow mesopores as well as pre-existing mesopores. As a consequence, the porosity of biochar samples increased, which is attributed to the increased surface area and pore volume of the biochar-800, as seen in Fig. 3B [59]. Table 1 reports the values of surface area, total and mesopores volume, and average pore diameter for different biochar samples. The higher surface area of biochar-800 is likely to improve the electrochemical charge storage performance of the supercapacitor by enhancing the capacitance, although the increased porosity could facilitate the transport of electrolyte ions within the pores of the supercapacitor during the operation.

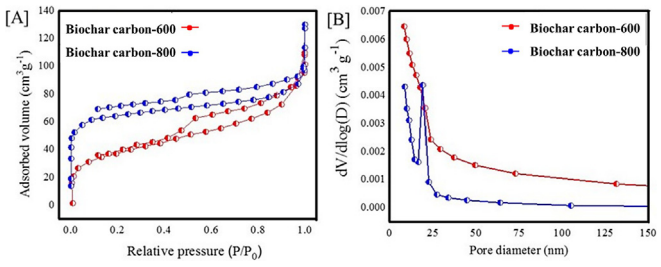

Fig. 3. [A] N_2 adsorption isotherm of biochar samples [B] Pore diameter and volume of biochar's.

3.4. Characterization of surface morphology and heteroatoms of biochar

To prepare the sample for TEM examination, 1 mg of biochar-800 powder was mixed with 1 ml of ethanol solution and sonicated for 15 min to obtain a homogeneous suspension. Later, 5 μl of the suspension was dropped on a 3.05 mm diameter Cu grid followed by drying under the I.R. lamp. The established porous structural features of biochar-800 were verified by TEM and high-resolution TEM analysis. The TEM analysis of biochar-800 revealed a hierarchical microporous feature of carbon, which facilitated the electrolyte ion transfer and decreased the resistance to ion diffusion (*cf.* Fig. 4[A] to [C]). The biochar-800 was identified as a composite of graphitic carbon rings assigned to the interlayer spacing of the (002) plan. Besides, the scanning transmission electron microscope-high-angle annular dark-field (STEM-HAADF) and its corresponding Energy-dispersive X-ray spectroscopy (EDS) elemental mapping images revealed the presence of heteroatoms and metal elements (Fig. 4[D] to [J]). The elemental mapping images exhibited the homogeneous distribution of C, N, O, effectively incorporated into the carbon structure and uniformly distributed in biochar-800 at the nanoscale. The presence of Ca, Fe, and Si elements was likely due to the dust particles attached to the biomass during the collection and palletization process, which interestingly enhanced the electrical conductivity of the biochar-800. The corresponding selected area electron diffraction (SAED) pattern exhibited the blurred diffraction ring, and it is assigned to the disorder or defected carbon structure, which could provide more adsorption sites to improve the capacitance performance (*cf.* Fig. 4[K]).

3.5. Characterization of surface composition of biochar

The XPS analysis revealed the chemical composition and chemical interaction/binding energy of the surface functional groups of biochar-800. The biochar-800 survey spectrum showed the presence of carbon (C), nitrogen (N), and oxygen (O) elements, indicating the self-doping heteroatoms within the biochar structure, as shown in Fig. 5[A]. The high-resolution spectra of C 1s are deconvoluted into four different binding energies viz. 284.7 eV, 285.4 eV, 287.1 eV, and 289 eV corresponding to C–C, C–N, C–O, and C = O species, respectively (*cf.* Fig. 5[B]). The C–C bond at 284.7 eV indicated that most of the sp^2 carbon atoms in biochar-800 are arranged in a conjugated honeycomb lattice. It was observed that binding energy acquired by C–C remained higher than the rest of the bond in the C 1s spectrum [60].

Further, the high-resolution spectrum of N 1s was divided into three constituent peaks: 399.8 eV, 400.5 eV, and 401.19 eV,

Table 1. S
Surface area, pore volumes, and average pore diameter of biochar samples

Sample name	S_{BET} (m^2 g^{-1})	Total pore volume (V_{tot}) cm^3 g^{-1}	Mesopores volume cm^3 g^{-1}	Average pore size (nm)
Biochar-600	199.1	28.18	0.0613	23.45
Biochar-800	312	43.95	0.143	15.12

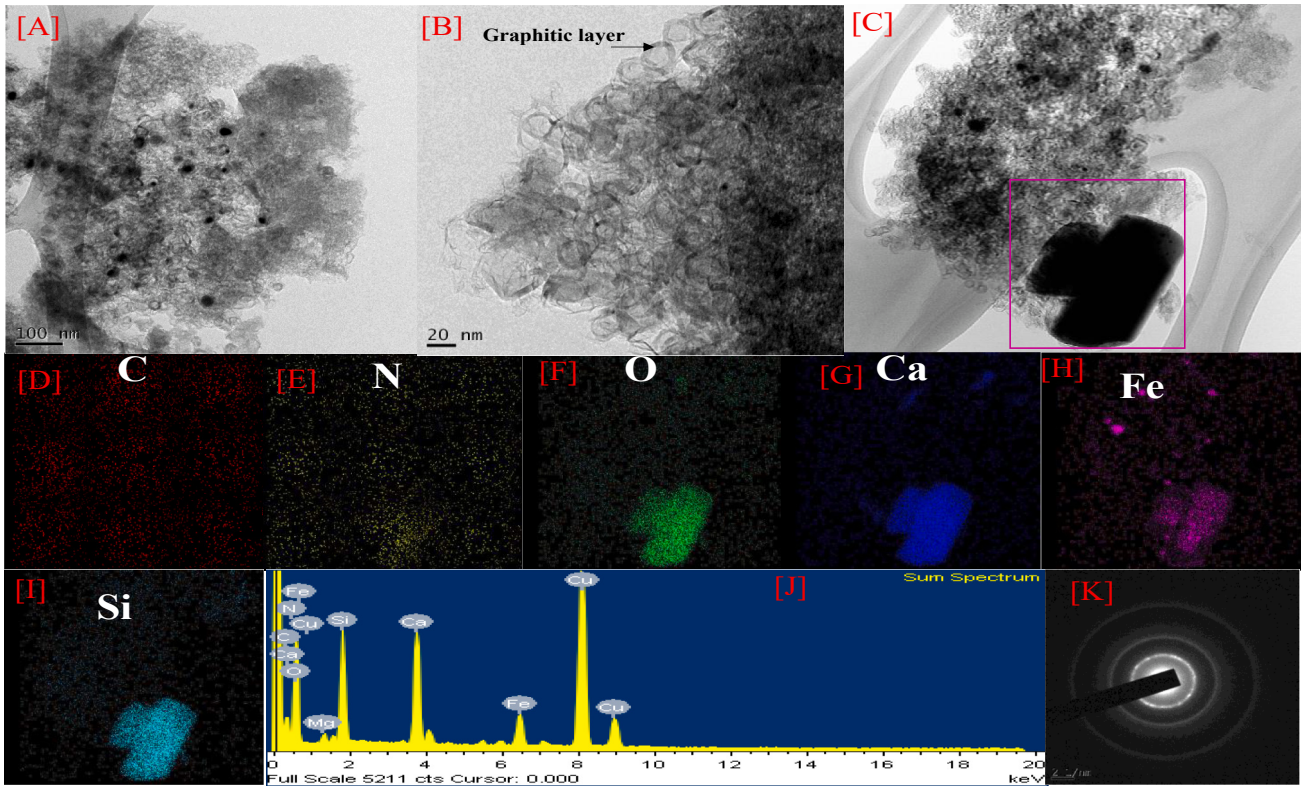

Fig. 4. [A] to [C] HR-TEM images of biochar-800 [D to J] STEM image and corresponding EDX elemental mapping of biochar-800 [K] SAED pattern of biochar-800.

assigned to the pyridine N (N-6), pyrrolic N (N-5), and quaternary N (N-Q), making a contribution of lone pair of the electron to the conjugated carbon, as depicted in Fig. 5[C] [61,62]. N-Q exhibited the ability of the electron donor and promoted the electron transfer kinetics. However, N-5 and N-6 were considered to contribute pseudo capacitance because it was situated at the edge of the C site [63,64]. Therefore, increased N-content, particularly N-5 and N-6 peak intensity, remained an effective strategy to enhance hydrophilicity and capacitance of the carbon-based electrode [65,66]. It is worth noting that the nitrogen in the graphitic carbon matrix of biochar possesses higher binding energy (401.19 eV) and active nature than the rest of the nitrogen (Fig. 5[D]). Moreover, the deconvoluted O 1s spectrum showed the binding energy as 533.4 eV and 536.3 eV, which corresponded to the single-bond of oxygen with carbon (i.e., C–O and C–O.H. groups, O-II), while double-bound of oxygen with carbon (i.e., C = O group, O-I) was observed at 532.2 eV. Further, the peak intensity observed at 536.3 eV can be attributed to carboxylic or chemisorbed oxygen or water (i.e., O = C–O group, O-III) [67,68]. The presence of oxygen-containing functional groups promoted the electrolyte ion's penetration into the biochar nanopores and enhanced the surface wettability. The surface composition analysis of the biochar samples via XPS thus revealed several key species responsible for supercapacitor performance. The schematic representation of the N and O co-doped carbon matrix, which played a crucial role in deciding electrochemical behavior, is represented in Fig. 5[E].

4. Electrochemical performance of biochar

4.1. Specific capacitance and galvanostatic charging-discharging (GCD) behavior of biochar

The supercapacitor study of the heteroatom-rich biochar was examined using a two-electrode system in 1 M H_2SO_4. The CV measurement of biochar-600 and biochar-800 was performed at a scan rate of 50 mVs^{-1} to evaluate the electrochemical kinetics of the electrode (*cf.* Fig. 6[A]). A couple of very well-defined redox peaks between 100 mV and 300 mV were distinctly seen from the CV curves of biochar-600 and biochar-800, which emerged primarily from the reversible faradic redox reaction associated with the presence of heteroatoms in the carbon structure of biochar. These heteroatoms remained electrochemically active, and the CV curve showed assertive pseudocapacitive behavior [69,70]. Even at a higher scan rate of 50 mVs^{-1}, the biochar-800 showed an excellent redox peak and its large enclosure area relative to the biochar-600, which suggests that at the higher temperature, the prepared material could possess a comparatively greater specific surface and hence higher specific capacitance.

Furthermore, the comparative galvanostatic charging-discharging (GCD) performance of the biochar-600 and biochar-800 as shown in Fig. 6[B]. The specific capacitance calculated from the discharging curve of biochar-600 and biochar-800 was 206F g^{-1} and 228F g^{-1}, respectively, which can be assigned to an increased specific surface area at a higher temperature and the

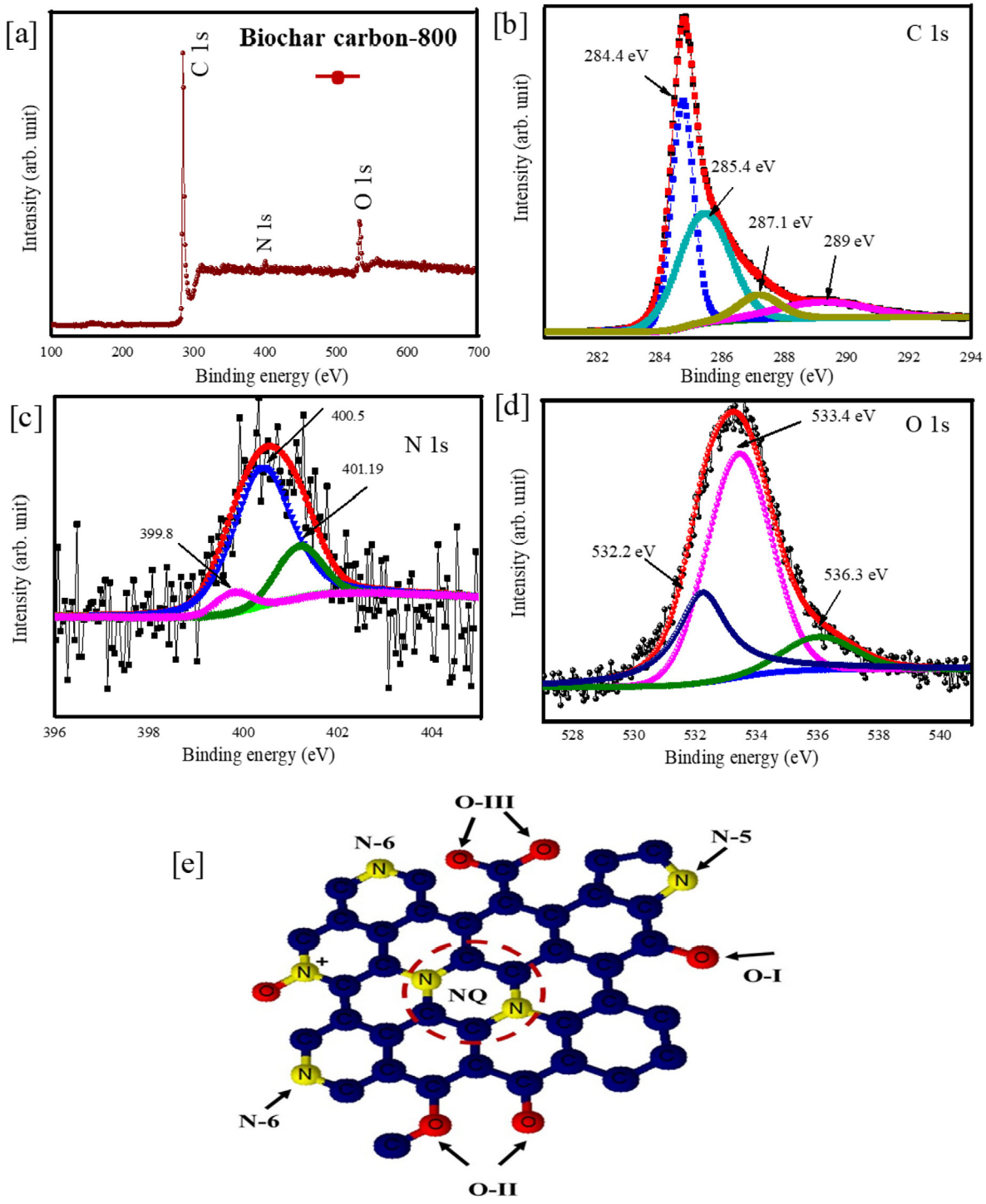

Fig. 5. [A] XPS survey scan spectra of the biochar-800 and high-resolution scan of [B-D] C 1s, N 1s, and O 1s [E] Schematic representation of different N and O functionalities.

slightly distorted triangular shape of the GCD curve, which confirm the pseudocapacitance nature of the biochar. In addition, using equation (2), the measured energy density at 1 A g^{-1} for biochar-600 and biochar-800 was determined as 7.27 Wh kg^{-1} and 7.91 Wh kg^{-1}, respectively. In two-electrode measurements, biochar-800 exhibited higher or comparable specific capacitance to the previously mentioned biomass-derived nanostructured biochar summarized in Table 2. No activation reagent is required in the synthesis of biochar-800 to increase the surface area of the material, which gives it an edge over other materials and lowers the processing cost of the biochar-800.

The electrochemical impedance spectroscopy (EIS) measurement was carried out in a 0.01 Hz to 0.1 GHz frequency window to evaluate the electrode/electrolyte interface, which triggered the overall impedance of the supercapacitor. In a Nyquist plot Fig. 6[C], the point where the plot intersects the real axis (x-axis) refers to equivalent series resistance (ESR), also known as the solution resistance (R_s), which was found as 3.4 Ω and 3.49 Ω, respectively, for biochar-600 and biochar-800 samples. The slight increase in the ESR value of biochar-800 is assigned to the increased pyrolysis temperature, making the biochar surface more hydrophobic and reducing the contact area at the electrode-

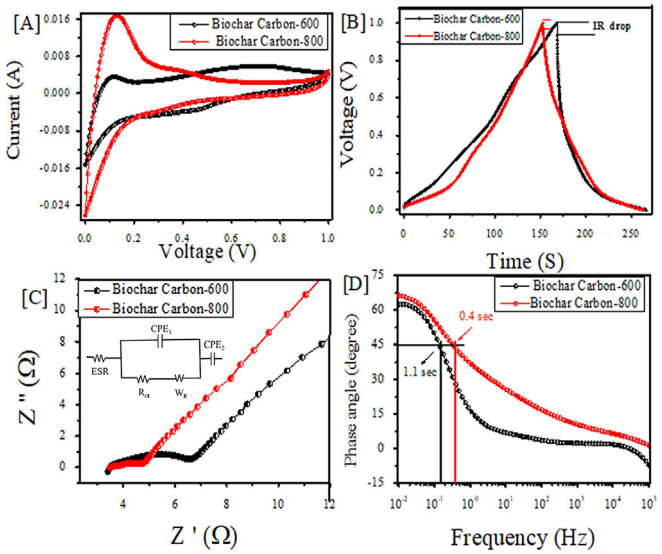

Fig. 6. [A] Cyclic voltammogram of biochar-600 and biochar-800 at a scan rate of 50 mVs^{-1} in 1M H_2SO_4, [B] GCD curve of biochar-600 and biochar-800 at a current density of 1 A g^{-1}, [C] Nyquist plot of biochar-600 and biochar-800 samples (inset shows the electrochemical equivalent circuit), [D] Bode plots of biochar-600 and biochar-800 samples

electrolyte interface. This electrode also exhibited a nearly vertical line in the low-frequency region, suggesting a good capacitive performance. Extrapolating the vertical portion (low-frequency area) to the real axis yields the total cell resistance (R_{cell}). Notably, the biochar-800 showed lower R_{cell} (4.9 Ω) compared to the biochar-600 (6.9 Ω), due to its lower charge transfer resistance (R_{CT}). The semicircle region of Fig. 6[C] revealed electrochemical reaction impedance of the electrode, while the smaller diameter of the semicircle denoted lower R_{CT}. Nyquist plot suggested that the biochar-800 had a smaller arc radius than biochar-600, confirming the fast electric response with the lowest R_{CT} value of 1.3 Ω compared to biochar-600 (3.24 Ω), which suggested the promotion of charge transfer in the case of biochar-800. The Warburg resistance (W_R) is estimated by subtracting R_{CT} and ESR from the R_{cell} value, and it remained as 0.27 Ω and 0.12 Ω for biochar-600 and biochar-800, respectively. Thus, the smaller R_{CT} and W_R values of biochar-800 indicated better charge transfer and ion penetration, resulting in excellent rate performance.

Fig. 6[D] demonstrates the Bode phase plots of the impedance phase angle vs. frequency obtained from the EIS plot. Since the capacitive and resistive impedances are identical at a phase angle of − 45°, the relaxation time constant (τ) can be calculated by $\tau = \frac{1}{f}$ at the particular phase. The relaxation time shows how fast the stored energy of the electrode can effectively be distributed. The phase angles are close to − 90° at low frequencies, suggesting ideal capacitive behavior. The biochar-800 showing the maximum phase angle of − 66° at the low-frequency region can be assigned to the capacitive behavior; the phase angle remained less than that of an ideal capacitive nature − 90°, demonstrating the pseudocapacitive nature of the electrode material [71]. The characteristic frequencies (f) for a phase angle of − 45° are 0.186 Hz and 0.48 Hz, corresponding to the relaxation time constant of 5.3 s and 2.0 s for biochar-600 and biochar-800, respectively. As the pyrolysis temperature increased, the diffusion coefficient of electrolyte in biochar-800 increased due to the high specific surface area, electrical conductivity, and mesopores structure. The mass transfer process and electrochemical reversibility of the biochar-800 were also improved with more prominent capacitive characteristics.

4.2. CV characteristic, internal resistance, and cycling stability of biochar

The CV measurement of the biochar-600 and biochar-800 samples at different scan rates from 10 mVs^{-1} to 150 mVs^{-1} and between 0.0 V and 1.0 V is demonstrated in Fig. 7[A] and [B]. Fig. 7[A] and [B] show that as the scan rate increased, the oxidation and reduction peaks of biochar-600 and biochar-800 shifted towards more positive and then negative values, primarily due to polarization and ohm resistance during the faradic processes. Similarly, as pyrolysis temperature increased (or from biochar-600 to biochar-800), slight improvements in the shape of the CV curves of biochar-800 were observed, such as the increase in the CV curve area and current density, which resulted in superior capacitance value. Dunn's power law equation was adapted to define the energy storage mechanism of biochar-600 and biochar-800, respectively, where the relationship between measured current (i) and scan rate (v) dependent equation is given as [81].

$$i = a.v^{b} \tag{3}$$

Where 'b' represents the adjustable parameter, which can be obtained from the slope of the plot of log (i) vs. log (v) at particular potential, as shown in Fig. 7[C] and [D]. A value of b = 0.5 is related to the diffusion-controlled Faradic process, while b = 1 implies to the capacitive (i.e., non –faradic) process. Futher, a value of b between 0.5 and 1 suggests an integrated process (i.e., faradic and non-faradic process). Fig. 7[C] and [D] exhibit that the 'b' value for biochar-600 and biochar-800 for anodic and cathodic peaks remained at 0.53, 0.63, and 0.51, 0.87, respectively, suggesting that the energy storage is a combination of diffusion-controlled and charge storage process which conformed the pseudocapacitive contribution[82]. Fig. 7[E] and [F] show the GCD curve at the different current density from 1 A $g^{-1}$to the 5 A g^{-1}. As current density increased, the internal resistance (I.R.) drop increased sharply due to the electrolyte's enhanced ionic motion velocity over a short period which posed difficulty for the electrolyte ions to penetrate within the pores of the biochar material. At 1 A g^{-1}, the biochar-

Table 2
Two electrode-specific capacitance measurements of electrode prepared by using various biomass-derived biochar

Biomass	Activation agent	S_{BET} (m^2g^{-1})	Electrolyte	Specific capacitance (F g^{-1})	Current density (A g^{-1})	Ref.
Phonex tree leaves	K_2FeO_4	2208	6 M KOH	254	0.5 A g^{-1}	[72]
Silkworm Cocoon	KOH	3386	6 M KOH	155.1	5 A g^{-1}	[73]
Tea waste	KOH	911.9	6 M KOH	167	1 A g^{-1}	[74]
Cotton	KOH	2307	6 M KOH	193	0.1–50 A g^{-1}	[75]
Lecithin	KOH	1803	1 M H_2SO_4	178	0.5 A g^{-1}	[76]
Soybean root	KOH	2143	6 M KOH	276	0.5 A g^{-1}	[77]
Dried Fungus	KOH	2959	6 M KOH	235	1 A g^{-1}	[78]
Bean dregs	KOH	2876	1 M H_2SO_4	210.2	1 A g^{-1}	[79]
Bagasse	KOH	1260	1 M H_2SO_4	225	1 A g^{-1}	[80]
Biochar-600	No-Activation	199.1	1 M H_2SO_4	206	1 A g^{-1}	Presentwork
Biochar-800	No-Activation	312	1 M H_2SO_4	228	1 A g^{-1}	Present work

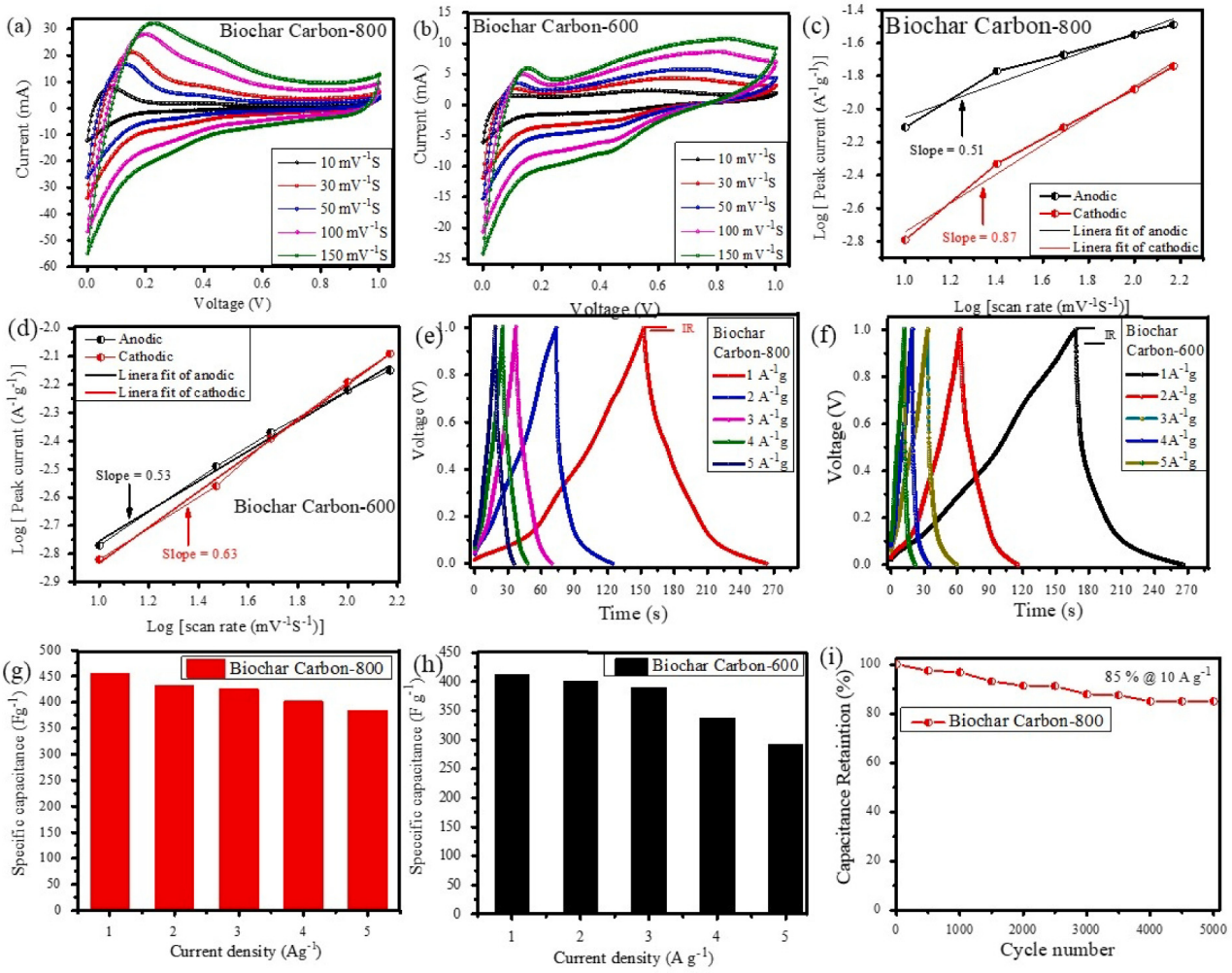

Fig. 7. [A – B] CV curve of biochar-600 and biochar-800 in a two-electrode system [C – D] log (i) vs log (v) plot at different scan rate [E – F], Galvanostatic charge-discharge curve of biochar-600 and biochar-800 [G – H] Specific capacitance at different current densities [I] Cyclic stability of biochar-800 at a constant current density of 10 $A^{-1}g$ up to 5000 cycles

600 showed an increased I.R. drop of 0.007 V compared to the biochar-800 (0.003 V). At a current density of 1 A g^{-1}, the biochar-800 exhibited a specific capacitance of 228F g^{-1} in a two-electrode cell. However, for an increase in the current density up to 5 A g^{-1}, the specific capacitance of biochar-800 retained up to 84 % as compared to biochar-600 (~70 %), as shown in Fig. 7[G] and [H]. The high specific capacitance retention % of biochar-800 can be attributed to the reduced internal charge transfer resistance, increased specific surface area, and mesopores at higher temperatures. The cycling stability of biochar-800 was examined by the GCD of the electrode between 0 V and 1 V. Fig. 7[I] shows that after 5000 charge–discharge cycles and at a high current density of 10 A g^{-1}, the capacitance retention % of biochar-800 remained near 88%, possibly due to the heteroatoms and porous carbon structures of biochar-800 which enabled access of electrolyte ions, and led to long-term cycling life and excellent reversibility of the biochar-800 electrode [83–85].

4.3. Application of biochar-800 as a coin cell supercapacitor

Fig. 8[A] shows a schematic of the coin cell device supercapacitor developed from biochar-800, as it showed the best electrochemical performance. The coin cell supercapacitor was

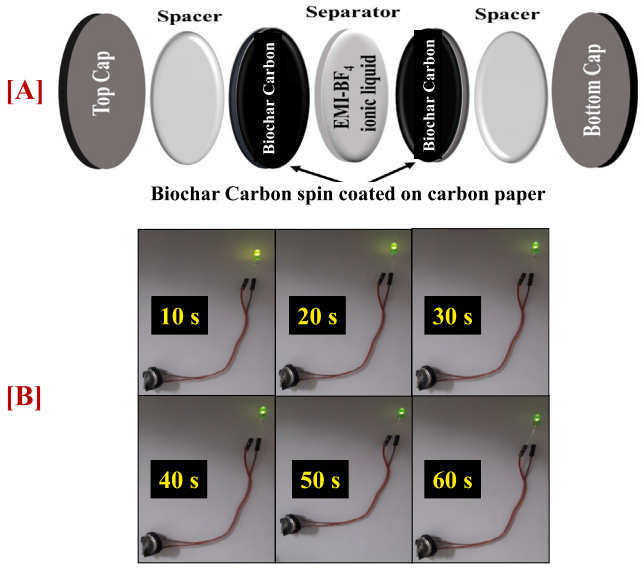

Fig. 8. [A] Schematic illustration of biochar-800-coin cell configuration, [B] Demonstration of working biochar-800-coin cell device glowing LED after the 30 s charging

constructed by spin coating 14 mg of biochar-800 slurry on conducting carbon paper containing 90 wt% of biochar-800, 5 wt% carbon black, and 5 wt% PVDF. The separator was placed between the electrodes after being immersed in 1-ethyl-3mthylimdazolium tetrafluoroborate (EMI-BF_4) ionic liquid as the electrolyte for a non-aqueous solution. The coin cell was pressed in a hydraulic coin cell crimping machine. The coin cell device was charged for the 30 s by applying 3 V; consequently, it glows 3 V LEDs for up to 60 s without any external power source Fig. 8[B]. The working of the coin cell device via video is demonstrated in the supporting information.

5. Conclusion

In summary, an electrode material was proposed and developed for symmetric pseudocapacitors with high specific capacitance and long cycling stability at higher current density. The prepared biochar exhibited N and O co-doped heteroatoms in the hierarchical porous carbon structure with a high micropore volume of 0.143 cm^3/gm. The biochar produced at 800 °C showed a specific capacitance of 228F g^{-1} at 1 A g^{-1} in 1 M H_2SO_4 and a rate capability of ~ 84.1% when current density increased up to 5 A g^{-1} (191.9F g^{-1}). Remarkably, the biochar-800 also showed an excellent energy density of 7.91 Wh kg^{-1} in 1 M H_2SO_4 electrolyte and improved cycling stability 88% capacitance retention after 5000 cycles at a high current density of 10 A g^{-1}. The increased specific capacitance is assigned to the existence of N and O co-doped heteroatoms within the graphitic carbon matrix of biochar, which enhanced the electrical conductivity, and ion adsorption on the surface, at ambient temperature. Furthermore, the low relaxation time constant, drop in the internal resistance, high specific surface area, and the presence of micropores played a crucial role in enhancing the electrochemical performance of biochar-800. Thus, the current study demonstrates that the low-cost co-doped heteroatoms rich hierarchical porous biochar material derived from the biomass pellets pyrolysis would be an excellent choice for a high-performance pseudocapacitive energy conversion device.

CRediT authorship contribution statement

Zakir Husain: Original work, methodology, data creation, and initial drafting. **A.R. Shakeelur Raheman:** Original work, methodology, data creation, and initial drafting. **Khursheed B. Ansari:** Conceptualization, mentoring and proofreading. **Aniruddha B. Pandit:** Supervision, project administration, funding acquisition. **Mohd Shariq Khan:** Critical comments and proofreading. **Muhammad Abdul Qyyum:** Critical comments and proofreading. **Su Shiung Lam:** Comments on supercapacitor.

Declaration of competing interest

The authors declare that they have no known competing financial interests or personal relationships that could have appeared to influence the work reported in this paper.

Acknowledgments

Zakir Husain and Shakeelur Rahman A. R. gratefully acknowledge the financial support from J.B. Joshi Research Foundation, MANF UGC ((F1-17.1/2013-14/MANF-2013-14-MUS-MAH-27907) , BRNS (2013/20/34/1/BRNS), and Nanomission (SR/NM/NS-1110/2012) Government of India. The authors would also like to thank Universiti Malaysia Terengganu under International Partnership Research Grant (UMT/CRIM/2-2/2/23 (23), Vot 55302), and the Ministry of Higher Education, Malaysia under the Higher Institution Centre of Excellence (HICoE), Institute of Tropical Aquaculture and Fisheries (AKUATROP) program (Vot. No. 63933 & Vot. No. 56051, UMT/CRIM/2-2/5 Jilid 2 (10)) for supporting Prof Lam to perform this joint project. The author would like to thank Dr. Sameer Patel (Department of Civil Engineering, Indian Institute of Technology, Gandhinagar, Gujarat, 382355, India) for his valuable suggestions on the manuscript.

Appendix A. Supplementary data

Supplementary data to this article can be found online at https://doi.org/10.1016/j.mset.2021.12.003.

References

[1] C. Zou, Q. Zhao, G. Zhang, B. Xiong, Energy revolution: From a fossil energy era to a new energy era, Natural Gas Industry B 3 (2016) 1–11.
[2] H.-F. Wang, Q. Xu, Materials Design for Rechargeable Metal-Air Batteries, Matter 1 (2019) 565–595.
[3] H. Iwahara, Conducting Materials: Solid-ionic and Super-ionic, in: K.H.J. Buschow, R.W. Cahn, M.C. Flemings, B. Ilschner, E.J. Kramer, S. Mahajan, P. Veyssière (Eds.), Encyclopedia of Materials: Science and Technology, Elsevier, Oxford, 2001, pp. 1482–1496.
[4] O.L. Li, T. Ishizaki, Chapter 4 – Development, Challenges, and Prospects of Carbon-Based Electrode for Lithium-Air Batteries, in: K.Y. Cheong, G. Impellizzeri, M.A. Fraga (Eds.), Emerging Materials for Energy Conversion and Storage, Elsevier, 2018, pp. 115–152.
[5] H. Yuan, H. Shimotani, J. Ye, S. Yoon, H. Aliah, A. Tsukazaki, M. Kawasaki, Y. Iwasa, Electrostatic and Electrochemical Nature of Liquid-Gated Electric-Double-Layer Transistors Based on Oxide Semiconductors, Journal of the American Chemical Society 132 (2010) 18402–18407.
[6] J. Walter, H. Wang, B. Luo, C.D. Frisbie, C. Leighton, Electrostatic versus Electrochemical Doping and Control of Ferromagnetism in Ion-Gel-Gated Ultrathin La0.5Sr0.5CoO3−δ, ACS Nano 10 (2016) 7799–7810.
[7] A. Gopalakrishnan, S. Badhulika, Effect of self-doped heteroatoms on the performance of biomass-derived carbon for supercapacitor applications, Journal of Power Sources 480 (2020) 228830.
[8] F. Zhao, A. Vicenzo, M. Hashempour, M. Bestetti, Supercapacitor electrodes by direct growth of multi-walled carbon nanotubes on Al: a study of performance versus layer growth evolution, Electrochimica Acta 150 (2014) 35–45.
[9] W. Ni, L. Shi, Review Article: Layer-structured carbonaceous materials for advanced Li-ion and Na-ion batteries: Beyond graphene, Journal of Vacuum Science & Technology A 37 (2019) 040803.
[10] A. Izadi-Najafabadi, S. Yasuda, K. Kobashi, T. Yamada, D.N. Futaba, H. Hatori, M. Yumura, S. Iijima, K. Hata, Extracting the Full Potential of Single-Walled Carbon Nanotubes as Durable Supercapacitor Electrodes Operable at 4 V with High Power and Energy Density, Advanced Materials 22 (2010) E235–E241.
[11] H. Zhang, X. He, J. Gu, Y. Xie, H. Shui, X. Zhang, N. Xiao, J. Qiu, Wrinkled porous carbon nanosheets from methylnaphthalene oil for high-performance supercapacitors, Fuel Processing Technology 175 (2018) 10–16.
[12] S. Zhang, L. Sui, H. Dong, W. He, L. Dong, L. Yu, High-Performance Supercapacitor of Graphene Quantum Dots with Uniform Sizes, ACS Applied Materials & Interfaces 10 (2018) 12983–12991.
[13] A. Castro-Muñiz, S. Lorenzo-Fierro, A. Martínez-Alonso, J.M.D. Tascón, V. Fierro, F. Suárez-García, J.I. Paredes, Ordered mesoporous carbons obtained from low-value coal tar products for electrochemical energy storage and water remediation, Fuel Processing Technology 196 (2019) 106152.
[14] C. Zhou, Y. Zhang, Y. Li, J. Liu, Construction of High-Capacitance 3D CoO@Polypyrrole Nanowire Array Electrode for Aqueous Asymmetric Supercapacitor, Nano Letters 13 (2013) 2078–2085.
[15] M. Zhi, F. Yang, F. Meng, M. Li, A. Manivannan, N. Wu, Effects of Pore Structure on Performance of An Activated-Carbon Supercapacitor Electrode Recycled from Scrap Waste Tires, ACS Sustainable Chemistry & Engineering 2 (2014) 1592–1598.
[16] H. Jiang, J. Ma, C. Li, Mesoporous Carbon Incorporated Metal Oxide Nanomaterials as Supercapacitor Electrodes, Advanced Materials 24 (2012) 4197–4202.
[17] R.R. Salunkhe, Y.V. Kaneti, Y. Yamauchi, Metal-Organic Framework-Derived Nanoporous Metal Oxides toward Supercapacitor Applications: Progress and Prospects, ACS Nano 11 (2017) 5293–5308.
[18] G.A. Snook, P. Kao, A.S. Best, Conducting-polymer-based supercapacitor devices and electrodes, Journal of Power Sources 196 (2011) 1–12.
[19] Y.-P. Gao, Z.-B. Zhai, K.-J. Huang, Y.-Y. Zhang, Energy storage applications of biomass-derived carbon materials: batteries and supercapacitors, New Journal of Chemistry 41 (2017) 11456–11470.
[20] Z. Hu, X. Li, Z. Tu, Y. Wang, O.D. Dacres, Y. Sun, M. Sun, H. Yao, "Thermal dissolution carbon enrichment" treatment of biomass wastes: Supercapacitor electrode preparation using the residue, Fuel Processing Technology 205 (2020) 106430.

[21] M. Khalid, A.M.B. Honorato, A.A. Pasa, H. Varela, A sugar derived carbon-red phosphorus composite for oxygen evolution reaction and supercapacitor activities, Materials Science for Energy Technologies 3 (2020) 508–514.
[22] P. Konnerth, D. Jung, J.W. Straten, K. Raffelt, A. Kruse, Metal oxide-doped activated carbons from bakery waste and coffee grounds for application in supercapacitors, Materials Science for Energy Technologies 4 (2021) 69–80.
[23] J.R. Miller, A.F. Burke, Electrochemical Capacitors: Challenges and Opportunities for Real-World Applications, The Electrochemical Society interface 17 (2008) 53–57.
[24] R. Farma, M. Deraman, A. Awitdrus, I.A. Talib, E. Taer, N.H. Basri, J.G. Manjunatha, M.M. Ishak, B.N.M. Dollah, S.A. Hashmi, Preparation of highly porous binderless activated carbon electrodes from fibres of oil palm empty fruit bunches for application in supercapacitors, Bioresource Technology 132 (2013) 254–261.
[25] M.M. Pérez-Madrigal, M.G. Edo, C. Alemán, Powering the future: application of cellulose-based materials for supercapacitors, Green Chemistry 18 (2016) 5930–5956.
[26] K. Subramani, N. Sudhan, M. Karnan, M. Sathish, Orange Peel Derived Activated Carbon for Fabrication of High-Energy and High-Rate Supercapacitors, ChemistrySelect 2 (2017) 11384–11392.
[27] L. Sun, C. Tian, M. Li, X. Meng, L. Wang, R. Wang, J. Yin, H. Fu, From coconut shell to porous graphene-like nanosheets for high-power supercapacitors, Journal of Materials Chemistry A 1 (2013) 6462–6470.
[28] J.-Q.-Q. Guo Pei-Zhi, Z.H.A.N.G. Li-Li, Z.H.A.O. Shan-Yu, Z.H.A.O. Xiu-Song, Preparation and Characterization of Peanut Shell-Based Microporous Carbons as Electrode Materials for Supercapacitors, Acta Phys. -Chim. Sin. 27 (2011) 2836–2840.
[29] M. Chen, X. Kang, T. Wumaier, J. Dou, B. Gao, Y. Han, G. Xu, Z. Liu, L. Zhang, Preparation of activated carbon from cotton stalk and its application in supercapacitor, Journal of Solid State Electrochemistry 17 (2013) 1005–1012.
[30] H. Wang, Z. Li, D. Mitlin, Tailoring Biomass-Derived Carbon Nanoarchitectures for High-Performance Supercapacitors, ChemElectroChem 1 (2014) 332–337.
[31] Y. Liu, J. Chen, B. Cui, P. Yin, C. Zhang, Design and Preparation of Biomass-Derived Carbon Materials for Supercapacitors: A Review, C 4 (2018) 53.
[32] H. Yang, S. Ye, J. Zhou, T. Liang, Biomass-Derived Porous Carbon Materials for Supercapacitor, Frontiers in Chemistry 7 (2019).
[33] G. Kandasamy, Recent Advancements in Doped/Co-Doped Carbon Quantum Dots for Multi-Potential Applications, C 5 (2019) 24.
[34] Y. Zhu, S. Murali, M.D. Stoller, K.J. Ganesh, W. Cai, P.J. Ferreira, A. Pirkle, R.M. Wallace, K.A. Cychosz, M. Thommes, D. Su, E.A. Stach, R.S. Ruoff, Carbon-Based Supercapacitors Produced by Activation of Graphene, Science 332 (2011) 1537–1541.
[35] D. Hulicova-Jurcakova, M. Seredych, G.Q. Lu, T.J. Bandosz, Combined Effect of Nitrogen- and Oxygen-Containing Functional Groups of Microporous Activated Carbon on its Electrochemical Performance in Supercapacitors, Advanced Functional Materials 19 (2009) 438–447.
[36] M. Seredych, D. Hulicova-Jurcakova, G.Q. Lu, T.J. Bandosz, Surface functional groups of carbons and the effects of their chemical character, density and accessibility to ions on electrochemical performance, Carbon 46 (2008) 1475–1488.
[37] Y. Zhao, M. Liu, X. Deng, L. Miao, P.K. Tripathi, X. Ma, D. Zhu, Z. Xu, Z. Hao, L. Gan, Nitrogen-functionalized microporous carbon nanoparticles for high performance supercapacitor electrode, Electrochimica Acta 153 (2015) 448–455.
[38] Z.R. Ismagilov, A.E. Shalagina, O.Y. Podyacheva, A.V. Ischenko, L.S. Kibis, A.I. Boronin, Y.A. Chesalov, D.I. Kochubey, A.I. Romanenko, O.B. Anikeeva, T.I. Buryakov, E.N. Tkachev, Structure and electrical conductivity of nitrogen-doped carbon nanofibers, Carbon 47 (2009) 1922–1929.
[39] D.-W. Wang, F. Li, H.-M. Cheng, Hierarchical porous nickel oxide and carbon as electrode materials for asymmetric supercapacitor, Journal of Power Sources 185 (2008) 1563–1568.
[40] B. Xu, S. Hou, G. Cao, F. Wu, Y. Yang, Sustainable nitrogen-doped porous carbon with high surface areas prepared from gelatin for supercapacitors, Journal of Materials Chemistry 22 (2012) 19088–19093.
[41] M. Yang, Z. Zhou, Recent Breakthroughs in Supercapacitors Boosted by Nitrogen-Rich Porous Carbon Materials, Advanced Science 4 (2017) 1600408.
[42] W. Qian, F. Sun, Y. Xu, L. Qiu, C. Liu, S. Wang, F. Yan, Human hair-derived carbon flakes for electrochemical supercapacitors, Energy & Environmental Science 7 (2014) 379–386.
[43] J. Lee, J. Oh, Y. Jeon, Y. Piao, Multi-Heteroatom-Doped Hollow Carbon Attached on Graphene Using LiFePO4 Nanoparticles as Hard Templates for High-Performance Lithium-Sulfur Batteries, ACS Applied Materials & Interfaces 10 (2018) 26485–26493.
[44] L. Zhang, J. Jiang, N. Holm, F. Chen, Mini-chunk biochar supercapacitors, Journal of Applied Electrochemistry 44 (2014) 1145–1151.
[45] C. Zequine, C.K. Ranaweera, Z. Wang, S. Singh, P. Tripathi, O.N. Srivastava, B.K. Gupta, K. Ramasamy, P.K. Kahol, P.R. Dvornic, R.K. Gupta, High Per formance and Flexible Supercapacitors based on Carbonized Bamboo Fibers for Wide Temperature Applications, Scientific Reports 6 (2016) 31704.
[46] Y. Wang, Y. Zhang, L. Pei, D. Ying, X. Xu, L. Zhao, J. Jia, X. Cao, Converting Ni-loaded biochars into supercapacitors: Implication on the reuse of exhausted carbonaceous sorbents, Scientific Reports 7 (2017) 41523.
[47] J. Jiang, High Temperature Monolithic Biochar Supercapacitor Using Ionic Liquid Electrolyte, Journal of The Electrochemical Society 164 (2017) H5043–H5048.
[48] E. Adhamash, R. Pathak, Q. Qiao, Y. Zhou, R. McTaggart, Gamma-radiated biochar carbon for improved supercapacitor performance, RSC Advances 10 (2020) 29910–29917.
[49] R.A. Senthil, V. Yang, J. Pan, Y. Sun, A green and economical approach to derive biomass porous carbon from freely available feather finger grass flower for advanced symmetric supercapacitors, Journal of Energy Storage 35 (2021) 102287.
[50] H. Wang, H. Yi, X. Chen, X. Wang, Asymmetric supercapacitors based on nano-architectured nickel oxide/graphene foam and hierarchical porous nitrogen-doped carbon nanotubes with ultrahigh-rate performance, Journal of Materials Chemistry A 2 (2014) 3223–3230.
[51] A. Ariharan, B. Viswanathan, V. Nandhakumar, Nitrogen-incorporated carbon nanotube derived from polystyrene and polypyrrole as hydrogen storage material, International Journal of Hydrogen Energy 43 (2018) 5077–5088.
[52] S.R. Mangisetti, M. Kamaraj, R. Sundara, Green Approach for Synthesizing Three Different Carbon Microstructures from a Single Biowaste Bombax malabaricum for Fully Biocompatible Flexible Supercapacitors and Their Performance in Various Electrolytes, ACS Omega 4 (2019) 6399–6410.
[53] T. Li, X. Bai, Y.-X. Qi, N. Lun, Y.-J. Bai, Fe3O4 nanoparticles decorated on the biochar derived from pomelo pericarp as excellent anode materials for Li-ion batteries, Electrochimica Acta 222 (2016) 1562–1568.
[54] L. Wang, C. Yang, S. Dou, S. Wang, J. Zhang, X. Gao, J. Ma, Y. Yu, Nitrogen-doped hierarchically porous carbon networks: synthesis and applications in lithium-ion battery, sodium-ion battery and zinc-air battery, Electrochimica Acta 219 (2016) 592–603.
[55] W. Qian, J. Zhu, Y. Zhang, X. Wu, F. Yan, Condiment-Derived 3D Architecture Porous Carbon for Electrochemical Supercapacitors, Small 11 (2015) 4959–4969.
[56] Y. Wang, Y. Song, Y. Wang, X. Chen, Y. Xia, Z. Shao, Graphene/silk fibroin based carbon nanocomposites for high performance supercapacitors, Journal of Materials Chemistry A 3 (2015) 773–781.
[57] M. Kruk, M. Jaroniec, Gas Adsorption Characterization of Ordered Organic−Inorganic Nanocomposite Materials, Chemistry of Materials 13 (2001) 3169–3183.
[58] G. Pognon, T. Brousse, D. Bélanger, Effect of molecular grafting on the pore size distribution and the double layer capacitance of activated carbon for electrochemical double layer capacitors, Carbon 49 (2011) 1340–1348.
[59] S. Gao, K. Geng, H. Liu, X. Wei, M. Zhang, P. Wang, J. Wang, Transforming organic-rich amaranthus waste into nitrogen-doped carbon with superior performance of the oxygen reduction reaction, Energy & Environmental Science 8 (2015) 221–229.
[60] C. Zhan, X. Yu, Q. Liang, W. Liu, Y. Wang, R. Lv, Z.-H. Huang, F. Kang, Flour food waste derived activated carbon for high-performance supercapacitors, RSC Advances 6 (2016) 89391–89396.
[61] C. Zhu, J. Zhai, S. Dong, Bifunctional fluorescent carbon nanodots: green synthesis via soy milk and application as metal-free electrocatalysts for oxygen reduction, Chemical Communications 48 (2012) 9367–9369.
[62] Z.-Y. Sui, Y. Cui, J.-H. Zhu, B.-H. Han, Preparation of Three-Dimensional Graphene Oxide-Polyethylenimine Porous Materials as Dye and Gas Adsorbents, ACS Applied Materials & Interfaces 5 (2013) 9172–9179.
[63] T. Lin, I.W. Chen, F. Liu, C. Yang, H. Bi, F. Xu, F. Huang, Nitrogen-doped mesoporous carbon of extraordinary capacitance for electrochemical energy storage, Science 350 (2015) 1508–1513.
[64] L. Zhang, T. You, T. Zhou, X. Zhou, F. Xu, Interconnected Hierarchical Porous Carbon from Lignin-Derived Byproducts of Bioethanol Production for Ultra-High Performance Supercapacitors, ACS Applied Materials & Interfaces 8 (2016) 13918–13925.
[65] W. Luo, B. Wang, C.G. Heron, M.J. Allen, J. Morre, C.S. Maier, W.F. Stickle, X. Ji, Pyrolysis of Cellulose under Ammonia Leads to Nitrogen-Doped Nanoporous Carbon Generated through Methane Formation, Nano Letters 14 (2014) 2225–2229.
[66] T. Liu, T. Kou, D. Bulmahn, C. Ortuno-Quintana, G. Liu, J.Q. Lu, Y. Li, Tuning the Electrochemical Properties of Nitrogen-Doped Carbon Aerogels in a Blend of Ammonia and Nitrogen Gases, ACS Applied Energy Materials 1 (2018) 5043–5053.
[67] M. Demir, B. Ashourirad, J.H. Mugumya, S.K. Saraswat, H.M. El-Kaderi, R.B. Gupta, Nitrogen and oxygen dual-doped porous carbons prepared from pea protein as electrode materials for high performance supercapacitors, International Journal of Hydrogen Energy 43 (2018) 18549–18558.
[68] S. Hu, Y. Tan, C. Feng, S. Wang, Z. Sun, H. Wu, G. Zhang, Improving biomass-derived carbon with cobalt/cobalt oxide doping for oxygen reduction reaction, Journal of Solid State Electrochemistry 23 (2019) 2291–2299.
[69] D.-D. Zhou, W.-Y. Li, X.-L. Dong, Y.-G. Wang, C.-X. Wang, Y.-Y. Xia, A nitrogen-doped ordered mesoporous carbon nanofiber array for supercapacitors, Journal of Materials Chemistry A 1 (2013) 8488–8496.
[70] E. Frackowiak, Carbon materials for supercapacitor application, Physical Chemistry Chemical Physics 9 (2007) 1774–1785.
[71] G.K. Veerasubramani, K. Krishnamoorthy, P. Pazhamalai, S.J. Kim, Enhanced electrochemical performances of graphene based solid-state flexible cable type supercapacitor using redox mediated polymer gel electrolyte, Carbon 105 (2016) 638–648.
[72] J. He, D. Zhang, Y. Wang, J. Zhang, B. Yang, H. Shi, K. Wang, Y. Wang, Biomass-derived porous carbons with tailored graphitization degree and pore size distribution for supercapacitors with ultra-high rate capability, Applied Surface Science 515 (2020) 146020.

[73] J. Sun, J. Niu, M. Liu, J. Ji, M. Dou, F. Wang, Biomass-derived nitrogen-doped porous carbons with tailored hierarchical porosity and high specific surface area for high energy and power density supercapacitors, Applied Surface Science 427 (2018) 807–813.
[74] X. Song, X. Ma, Y. Li, L. Ding, R. Jiang, Tea waste derived microporous active carbon with enhanced double-layer supercapacitor behaviors, Applied Surface Science 487 (2019) 189–197.
[75] P. Cheng, T. Li, H. Yu, L. Zhi, Z. Liu, Z. Lei, Biomass-Derived Carbon Fiber Aerogel as a Binder-Free Electrode for High-Rate Supercapacitors, The Journal of Physical Chemistry C 120 (2016) 2079–2086.
[76] M. Demir, S.K. Saraswat, R.B. Gupta, Hierarchical nitrogen-doped porous carbon derived from lecithin for high-performance supercapacitors, RSC Advances 7 (2017) 42430–42442.
[77] N. Guo, M. Li, Y. Wang, X. Sun, F. Wang, R. Yang, Soybean Root-Derived Hierarchical Porous Carbon as Electrode Material for High-Performance Supercapacitors in Ionic Liquids, ACS Applied Materials & Interfaces 8 (2016) 33626–33634.
[78] K. Wang, M. Xu, Z. Gu, P. Ahrenkiel, J. Lee, W. Gibbons, J. Croat, Q. Fan, Pyrrole modified biomass derived hierarchical porous carbon as high performance symmetrical supercapacitor electrodes, International Journal of Hydrogen Energy 41 (2016) 13109–13115.
[79] C. Ruan, K. Ai, L. Lu, Biomass-derived carbon materials for high-performance supercapacitor electrodes, RSC Advances 4 (2014) 30887–30895.
[80] M. Wahid, D. Puthusseri, D. Phase, S. Ogale, Enhanced Capacitance Retention in a Supercapacitor Made of Carbon from Sugarcane Bagasse by Hydrothermal Pretreatment, Energy & Fuels 28 (2014) 4233–4240.
[81] W. Sun, G. Gao, Y. Du, K. Zhang, G. Wu, A facile strategy for fabricating hierarchical nanocomposites of V2O5 nanowire arrays on a three-dimensional N-doped graphene aerogel with a synergistic effect for supercapacitors, Journal of Materials Chemistry A 6 (2018) 9938–9947.
[82] H.B. Li, M.H. Yu, F.X. Wang, P. Liu, Y. Liang, J. Xiao, C.X. Wang, Y.X. Tong, G.W. Yang, Amorphous nickel hydroxide nanospheres with ultrahigh capacitance and energy density as electrochemical pseudocapacitor materials, Nature Communications 4 (2013) 1894.
[83] L. Cao, H. Li, Z. Xu, H. Zhang, L. Ding, S. Wang, G. Zhang, H. Hou, W. Xu, F. Yang, S. Jiang, Comparison of the heteroatoms-doped biomass-derived carbon prepared by one-step nitrogen-containing activator for high performance supercapacitor, Diamond and Related Materials 114 (2021) 108316.
[84] J. Wang, Y. Xu, M. Yan, B. Ren, X. Dong, J. Miao, L. Zhang, X. Zhao, Z. Liu, Preparation and application of biomass-based porous carbon with S, N, Zn, and Fe heteroatoms loading for use in supercapacitors, Biomass and Bioenergy 156 (2022) 106301.
[85] H. Quan, X. Fan, W. Wang, W. Gao, Y. Dong, D. Chen, Hierarchically porous carbon derived from biomass: Effect of mesopore and heteroatom-doping on electrochemical performance, Applied Surface Science 460 (2018) 8–16.